Journal of Structural Geology 33 (2011) 1122–1134

Contents lists available at ScienceDirect

Journal of Structural Geology

journal homepage: www.elsevier.com/locate/jsg

Shear-induced graphitization of carbonaceous materials during seismic fault motion: Experiments and possible implications for fault mechanics

Kiyokazu Oohashi [a,*], Takehiro Hirose [b], Toshihiko Shimamoto [a,1]

[a] Department of Earth and Planetary Systems Science, Graduate School of Science, Hiroshima University, Higashi-Hiroshima 739-8526, Japan
[b] Kochi Institute for Core Sample Research, Japan Agency for Marine-Earth Science and Technology (JAMSTEC), Kochi 783-8502, Japan

ARTICLE INFO

Article history:
Received 29 September 2010
Received in revised form
6 January 2011
Accepted 10 January 2011
Available online 19 January 2011

Keywords:
Seismic fault
Carbonaceous materials
Graphite
Fault gouge
Friction experiment
Fault weakening

ABSTRACT

Carbonaceous materials often concentrate in fault zones developed in pelitic rocks. Among carbonaceous minerals, graphite is known as a lubricant and possibly plays a key role in frictional properties of the fault. Graphite reported from slip localized zones suggests that graphitization can occur during seismogenic fault motion. Thus, we performed friction experiments on amorphous carbon and graphite to investigate how graphite forms in association with fault motion and how these carbonaceous minerals affect frictional properties of faults. Experiments were done at normal stresses of 0.5–2.8 MPa and slip rates of 50 μm/s to 1.3 m/s in atmospheres of air and N_2 gas, using rotary-shear apparatuses. XRD and TEM analyses revealed that graphitization can indeed occur during seismogenic fault motion perhaps due to large shear strain, short-lived flash heating and stress concentration at asperity contacts, even at low temperatures and pressures under anoxic environments. We found large differences in steady-state friction coefficient μ_{ss} between graphite ($\mu_{ss} = 0.1$) and amorphous carbon ($\mu_{ss} = 0.54$) at low slip rate. But amorphous carbon exhibits marked velocity weakening at slip rate above 10 mm/s, and its steady-state friction reduces to the same level as that of graphite at a slip rate of 1.3 m/s. Faults with amorphous carbon are not weak at low slip rates, but they can become dynamically weak to foster fault motion during the generation of large earthquakes. Enriched graphite in fault zones can lubricate at all slip rates even at great depths and should receive more attention.

1. Introduction

Fault rocks enriched in carbonaceous materials (e.g., amorphous carbon and graphite) are reported from several fault zones, the Ushikubi fault (Oohashi and Kobayashi, 2008) and Tanakura Tectonic Line, Japan (Awaji, 2006), the KTB borehole, Germany (Zulauf et al., 1990), and the Err nappe detachment fault, Switzerland (Manatschal, 1999). These carbonaceous fault rocks are characteristically black and developed as ultracataclasite or fault gouge in the fault core. The outcrop shown in Fig. 1 is the Tanakura Western Marginal fault (the Inazawa outcrop; Awaji et al., 2010) with strike-slip displacement of more than a kilometer. The fault core mainly consists of foliated cataclasite and foliated fault gouge zones (G1, G2, and G3 in Fig. 1b). The matrix of these blackish gouge zones contains about 10 wt% of carbonaceous materials with particles <2 μm in size (arrows in Fig. 1d). Although the degree of graphitization varies among the three gouge layers, the greatest degree of crystallinity of carbonaceous materials is in the principal slip zone G1′ between the G2 and foliated fault gouge zone (Fig. 1c and e). Graphite is a well-known solid lubricant (e.g., Savage, 1948) and has potential to lubricate fault zones dramatically.

Tanakura carbonaceous gouge zones are incohesive fault rocks that moved at anoxic shallow depths, so that pressure and temperature conditions during the formation of this gouge zones are far below those estimated previously from the natural occurrence of graphite in metamorphic rocks (e.g., 300–500 °C and 400–500 MPa by Diessel et al., 1978; Buseck and Huang, 1985) and by laboratory experiments (e.g., 600–900 °C and 600 MPa by Oberlin, 1984; Nover and Stoll, 2001; Wilks et al., 1993; Bustin et al., 1995). We speculate that the graphite forms in response to frictional heat during coseismic slip. However, the graphitization processes along the fault zone and its mechanical response, especially at high slip rates, are not fully understood. Thus, the first problem we address in this paper is whether or not graphite can form in fault zones. We used commercial products of amorphous carbon and graphite as natural analogs to avoid complexities arising from natural carbonaceous materials with different degrees of crystallinity (e.g., Itaya, 1981). Low to high-velocity shearing experiments were conducted with those materials as simulated fault gouge, using two rotary-shear apparatuses (Shimamoto and Tsutsumi, 1994;

* Corresponding author. Tel.: +81 82 424 7469; fax: +81 82 424 0735.
E-mail address: kiyo-geologist@hiroshima-u.ac.jp (K. Oohashi).
[1] Present address: State Key Laboratory of Earthquake Dynamics, Institute of Geology, China Earthquake Administration, P.O. Box 9803, Beijing 100029, China.

0191-8141/$ – see front matter © 2011 Elsevier Ltd. All rights reserved.
doi:10.1016/j.jsg.2011.01.007

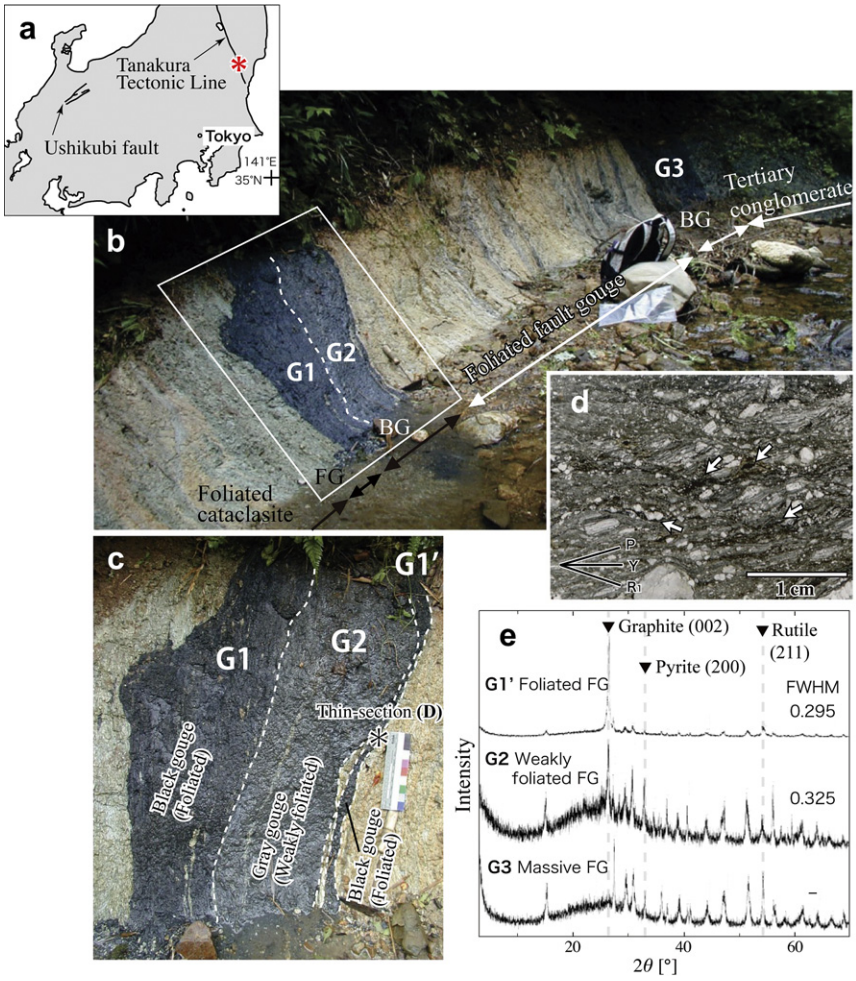

Fig. 1. Carbonaceous fault rock in the Tanakura Tectonic Line and its mineralogical features. (a) Index map showing the location of the outcrop (asterisk). (b) Photograph of the Inasawa outcrop of the Tanakura Western Marginal Fault (FG, fault gouge; BG, black fault gouge; G1, strongly foliated black fault gouge (slip localized zone); G2, weakly foliated gray fault gouge; G3, almost nonfoliated black fault gouge). (c) Closeup of the carbonaceous fault gouge. Narrow, highly deformed fault gouge G1′ (a few centimeters wide) is between G2 and the foliated gouge zone. We defined G1′ as the principal slip zone. (d) Plane-polarized light photograph of thin section of the G1′ fault gouge (XZ section). P, R_1, and Y denote the P-, R_1-, and Y-surfaces, respectively. (e) X-ray powder diffraction patterns of black fault gouge. Specimens were treated with hydrofluoric and hydrochloric acids for extraction of carbonaceous materials. The graphite corrected from G1′ gouge zone (principal slip zone) shows higher crystallinity than that of G2 and G3 gouge. FWHM: full width at half maximum of graphite (002) diffraction.

Shimamoto and Hirose, 2006). Our aims are twofold: (1) to determine if graphite forms from amorphous carbon during frictional sliding, and (2) to examine how frictional properties change from amorphous carbon to graphite at low to seismic slip rates.

Another interesting aspect of this study is the characterization of frictional properties for amorphous materials for a range of slip rates. Amorphous materials are known to form during friction experiments (Yund et al., 1990) and formation of silica gel or amorphous wet materials is suggested to cause dramatic fault weakening at intermediate to high slip rates (Goldsby and Tullis, 2002; Di Toro et al., 2004). High-velocity gouge experiments also produced amorphous materials in decomposed kaolinite (Brantut et al., 2008) due to frictional heating. Mineral decomposition during seismic fault motion was confirmed also by Han et al. (2007a,b) and Hirose and Bystricky (2007) although presence of amorphous materials was not reported. Formation of amorphous materials seems to be a widespread phenomenon in fault zones, but the mechanical properties of amorphous geomaterials have not been investigated systematically, except for coal (O'Hara et al., 2006). Thus, our experiments for amorphous carbon may provide insight into the possible role of amorphous materials on mechanical properties of fault zone.

2. Experimental procedures

We used two starting materials for simulated fault gouge: synthetic amorphous carbon powder (angular shape and grain size <45 μm, Strem Chemicals, Inc., product number 93-0601) and highly crystallized natural graphite (platy shape and grain size <45 μm, Wako Pure Chemical Industries, Ltd., product number 072-03845). Friction experiments were performed using a rotary-shear, high-velocity friction apparatus (HVR) at Kochi/JAMSTEC (Shimamoto and Tsutsumi, 1994; Hirose and Shimamoto, 2005) and a rotary-shear, low to high-velocity friction apparatus (HDR) at Hiroshima University (Shimamoto and Hirose, 2006). The experiments were conducted at normal stresses (σ_n) of 0.5–2.8 MPa, equivalent slip rates (V_e) of 50 μm/s to 1.3 m/s, and displacements of 0.09–118 m. Because the slip rate increases from the center to the periphery of the cylindrical specimens, we used the equivalent slip rate, V_e, defined such that $\tau V_e S$ gives the rate of total frictional work on a fault with area S, assuming a constant shear stress τ over the fault surface (Shimamoto and Tsutsumi, 1994). Hereafter, for convenience, we refer to "equivalent slip rate" as simply "slip rate" or "velocity".

Simulated fault gouge was placed between two cylinders of dolerite host rock with 25.0 mm diameters whose end surfaces

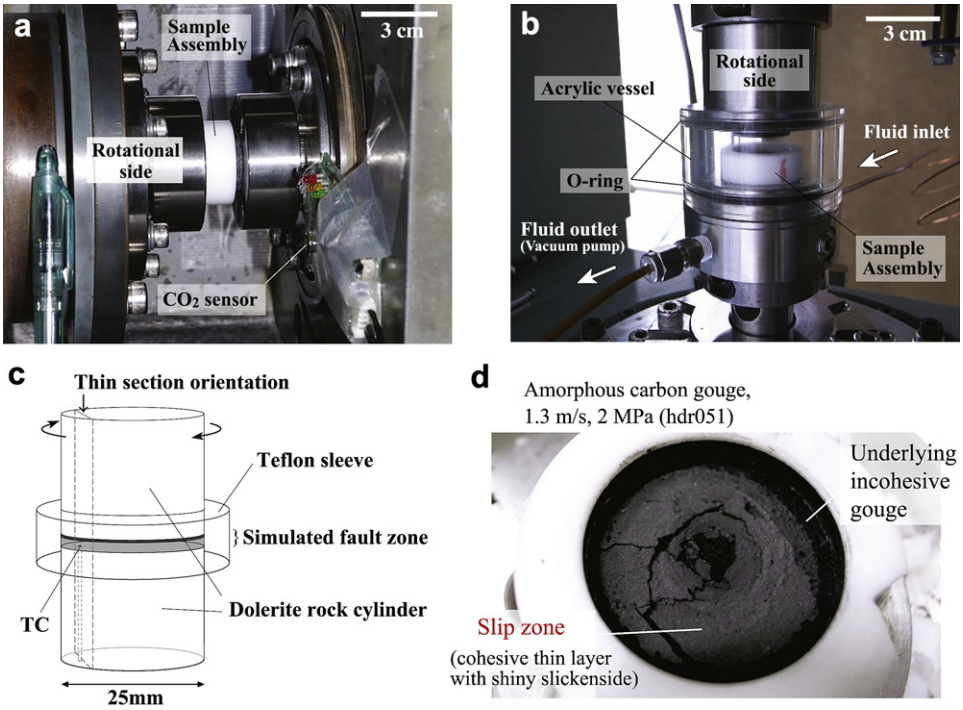

Fig. 2. (a) Photograph showing the specimen chamber of the HVR apparatus including placement of the CO_2 sensor. (b) Photograph of the acrylic vessel and specimen holder configuration of the HDR apparatus for experiments in a N_2 atmosphere. (c) Specimen configuration used in this study. Thin sections were made along the illustrated longitudinal section after the experiments. A thermocouple (TC) was placed 0.3 mm below the sliding surface in two experiments (hdr194, 195). (d) Slip surface of amorphous carbon gouge sheared at a slip rate of 1.3 m/s and normal stress of 2.0 MPa in a N_2 atmosphere (hdr051). The gouge from the cohesive thin layer was sampled for XRD analysis and TEM observation.

were ground with SiC 80# powder (see Fig. 2c). A Teflon sleeve of 24.9 mm in inner diameter was attached around the simulated fault zone to prevent gouge leakage. To correct for the effect of friction between the Teflon sleeve and the cylinders, we measured the shear traction caused by the sleeve in experiments without gouge, and then subtracted that traction from the measured raw data (see details in Appendix A). Thus, the effect of the Teflon sleeve is removed from the frictional data reported in this paper.

All starting materials and host rock cylinders were dried in an oven at 80 °C for at least 48 h before experiments. The experiments used 0.3 g of amorphous carbon or 0.5 g of highly crystallized graphite to provide a consistent gouge thickness at about 1 mm for all runs.

Experiments by the HDR apparatus were conducted under one of two atmospheric conditions: (1) in air at room temperature and humidity to simulate conditions near the ground, and (2) in dry nitrogen (N_2) gas to simulate anoxic environments such as deep crustal depths. All experiments by the HVR apparatus were done in air. To achieve the anoxic environment, we placed a small acrylic vessel around the sample holder of the HDR apparatus (Fig. 2b), evacuated it with a vacuum pump, and then charged it with N_2 gas, repeating this procedure three times before the experiment. We confirmed that relative humidity in the vessel was less than 2%, the detection limit of the sensor. Rubber O-rings were placed at the top and bottom of the acrylic vessel (Fig. 2b) to prevent gas leakage. The measured torque supported by the O-rings was <0.05 N/m, corresponding to shear stress of ~0.01 MPa. In some experiments (hdr194, 195; Table 1), a K-type (chromel–alumel type) thermocouple was placed 0.3 mm below the sliding surface to measure the temperature of the simulated fault zone.

In some experiments using the HVR apparatus, we examined the chemical transformation of carbon to CO_2 gas during the experiment by setting a solid electrolyte-type CO_2 sensor (TGS4161, Figaro Co. Ltd.) with response time of about 2 s. The sensor was placed approximately 50 mm away from the specimen holder (Fig. 2a). The experimental conditions and results are summarized in Table 1.

3. Mechanical behaviors

3.1. Representative slip behaviors

Fig. 3 shows a representative experimental result for amorphous carbon gouge subjected to a slip rate v of 1.3 m/s and normal stress σ_N of 1.4 MPa. Friction increased rapidly to an initial peak friction coefficient μ_p (0.56) and then decreased exponentially with displacement toward a steady-state friction coefficient μ_{ss} (0.12) over a slip-weakening distance D_c (12.9 m). This behavior can be described by an empirical equation (Mizoguchi et al., 2007; see dashed line in Fig. 3):

$$\mu = \mu_{ss} + \left(\mu_p - \mu_{ss}\right)\exp[\ln(0.05)(D/D_c)] \quad (1)$$

where D is the fault displacement after the peak friction and D_c is the slip-weakening distance over which $\mu - \mu_{ss}$ falls to 5% of $\mu_p - \mu_{ss}$. Experimental data for amorphous carbon were fit with this equation (Table 1).

For similar conditions (σ_n = 1.6 MPa and v = 1.3 m/s), graphite gouge showed very different behaviors with much smaller peak friction than for amorphous carbon and with friction remaining nearly constant (μ_{ss} = 0.08) without obvious slip-weakening or strengthening throughout the experiment (Fig. 3). We did not fit graphite data with Eq. (1).

Table 1
Summary of experimental data reported in this paper.

Run No.	Material	Atmospheric Condition	Velocity [m/s]	Normal Stress [MPa]	Displacement [m]	Peak Friction		Steady-state Friction			Dc [m]	Remarks				
						τ [MPa]	μ	τ [MPa]	Error	μ						
hvr1546	Graphite	Air	1.3	1.01	11.8	0.17	0.17	–	–	–	–	[c]				
hvr1549	Graphite	Air	1.3	1.0	47.95	[b]	–	0.09	±0.01	0.09	–					
hvr1555	Graphite	Air	0.87	1.0	83.28	[b]	–	0.1	±0.02	0.1	–	CO2 monitoring (Max: 40 ppm)				
hvr1558	Amorphous Carbon	N_2	1.3	1.0	16.2	0.70	0.70	0.15	±0.02	0.15±0.02	14.7					
hvr1561	Amorphous Carbon	Air	1.3	1.0	11.0	0.63	0.62	0.13	±0.02	0.19	38.2	CO2 monitoring (Max: 160-180 ppm)				
hvr1556	Graphite	Air	0.43	1.0	38.01	[b]	–	0.14	±0.02	0.13	–					
hvr1557	Graphite	Air	0.043	1.0	7.6	[b]	–	0.13	±0.01	0.13	–					
hvr1560	Amorphous Carbon	Air	1.3	1.0	22.0	0.59	0.59	0.18	±0.03	0.18	13.7	XRD measurement of recovered gouge				
hvr1564	Graphite	Air	1.3	1.0	43.8	[b]	–	0.12	±0.02	0.12±0.02	–	Slipping zone		Undeformed zone		
hdr050	Amorphous Carbon	N_2	1.3	1.0	17	0.52	0.52	0.17	±0.02	0.15±0.05	11.0	d002 [Å]	Int. [cps]	d002 [Å]	Int. [cps]	
hdr051	Amorphous Carbon	N_2	1.3	2.0	23.7	0.84	0.42	0.24	–	0.11	12	3.33	524	3.36	170	
hdr066-1	Amorphous Carbon	Air	0.04	1.0	2.94	0.57	0.57	0.57	±0.05	0.54±0.05	[a]					
hdr066-2	Amorphous Carbon	Air	0.009	1.85	17.13	1.0	0.56	1.0	±0.02	0.51±0.02	[a]	3.36?		No peak		
hdr114	Amorphous Carbon	N_2	0.009	2.0	15.0	[b]	–	0.87	±0.02	0.43±0.02	–					
hdr115	Amorphous Carbon	N_2	1.3	2.0	29.5	1.11	0.6	0.36	±0.03	0.19	2.5					
hdr116	Amorphous Carbon	N_2	1.3	1.4	32.6	0.78	0.56	0.17	±0.01	0.12	12.9					
hdr117	Amorphous Carbon	N_2	1.3	1.44	18.7	0.61	0.53	0.3	–	0.21	7.3					
hdr119	Amorphous Carbon	N_2	1.3	2.0	35.4	1.28	0.59	0.27	–	0.13	9.1					
hdr121	Amorphous Carbon	N_2	1.3	2.0	21.1	1.18	0.58	0.3	±0.05	0.15	6.39	3.35	230	No peak	–	
hdr124	Amorphous Carbon	N_2	1.3	2.0	33.4	1.07	0.58	0.3	±0.02	0.12±0.02	11.4	3.36	209	No peak	–	
hdr125	Amorphous Carbon	Air	1.3	2.0	27.3	1.1	0.55	0.24	±0.02	0.12	5.8	No peak	–	No peak	–	
hdr192	Amorphous Carbon	N_2	1.3	2.0	30.8	1.21	0.62	0.37	±0.02	0.18	6.7	3.34	464	No peak	–	
hdr193	Amorphous Carbon	N_2	1.3	2.8	28.2	1.42	0.51	0.46	–	0.16	4.2	3.35	223	3.35	160	
hdr194	Amorphous Carbon	Air	1.3	2.0	43.0	1.14	0.57	0.28	±0.05	0.12	12.7					TC
hdr195	Amorphous Carbon	N_2	1.3	2.0	31.3	1.13	0.59	0.40	±0.05	0.15	[a]	3.34	331	3.35	459	TC
hdr196	Amorphous Carbon	N_2	1.3	2.0	28.0	0.92	0.46	0.36	–	0.13	7.3					
hdr197	Amorphous Carbon	N_2	1.3	2.0	32.7	1.01	0.51	0.29	±0.03	0.15	9.2					
hdr198	Amorphous Carbon	N_2	1.3	2.0	30.6	0.95	0.47	0.24	±0.03	0.11	7.7					
hdr199	Amorphous Carbon	N_2	1.3	2.0	25.5	1.02	0.51	0.19	±0.005	0.09	10.45					
hvr2264	Amorphous Carbon	Air	0.00022	2.0	36.5	[b]	–	1.05	±0.04	0.53±0.02	–					
hdr623-0-1	Graphite	Air	0.00016	1.85	0.17	[b]	–	0.17	±0.02	0.09	–	No obvious peak		No obvious peak		
hdr623-0-2	Graphite	Air	0.00005	1.85	0.09	[b]	–	0.17	±0.05	0.09	–					
hdr623-0-3	Graphite	Air	0.0005	1.85	0.16	[b]	–	0.21	±0.01	0.11	–					
hdr623-0-4	Graphite	Air	0.001	1.85	0.16	[b]	–	0.23	±0.01	0.12	–					
hdr623-1	Graphite	Air	0.001	1.85	0.16	[b]	–	0.14	±0.01	0.08	–					
hdr623-2	Graphite	Air	0.004	1.85	1.14	[b]	–	0.16	±0.02	0.09	–					
hdr623-3	Graphite	Air	0.044	1.85	6.4	[b]	–	0.29	±0.01	0.16	–					
hdr623-4	Graphite	Air	0.13	1.85	13.0	[b]	–	0.15	±0.03	0.08	–					
hdr624-0	Graphite	Air	0.00005	1.85	0.05	[b]	–	0.27	±0.01	0.15	–					
hdr624-1	Graphite	Air	0.056	1.85	12.4	[b]	–	0.22	±0.01	0.12	–					
hdr624-2	Graphite	Air	0.056	1.85	6.36	[b]	–	0.19	±0.02	0.10	–					
hdr624-3	Graphite	Air	0.13	1.85	5.5	[b]	–			–	–					
hdr625	Graphite	Air	0.13	1.85	17.1	[b]	–	0.24	±0.01	0.13	–					
hdr626-0	Graphite	Air	0.436	1.85	17.0	[b]	–	0.25	±0.01	0.14	–					
hdr626-1	Graphite	Air	0.436	1.85	25.5	[b]	–			<0.20	–	[c]				
hdr627	Graphite	Air	0.436	1.85	20.8	[b]	–	0.22	±0.01	0.12	–					
hdr628	Graphite	Air	0.872	1.85	101	[b]	–	0.2	±0.01	0.11	–					
hdr629-0-1	Amorphous Carbon	Air	0.00005	1.84	0.10	[b]	–	0.99	±0.05	0.55	–					
hdr629-0-2	Amorphous Carbon	Air	0.0001	1.84	0.10	[b]	–	0.98	±0.02	0.54	–					
hdr629-0-3	Amorphous Carbon	Air	0.0005	1.84	0.21	[b]	–	1.01	±0.02	0.56	–					
hdr629-0-4	Amorphous Carbon	Air	0.001	1.84	0.36	[b]	–	1.02	±0.04	0.56	–					
hdr629-1-1	Amorphous Carbon	Air	0.005	1.84	0.8	1	0.59	0.96	±0.02	0.55	0.01					

(*continued on next page*)

Table 1 (*continued*)

Run No.	Material	Atmospheric Condition	Velocity [m/s]	Normal Stress [MPa]	Displacement [m]	Peak Friction		Steady-state Friction			Dc [m]	Remarks
						τ [MPa]	μ	τ [MPa]	Error	μ		
hdr629-1-2	Amorphous Carbon	Air	0.009	1.84	2.1	0.97	0.58	0.9	±0.02	0.51	0.9	
hdr629-1-3	Amorphous Carbon	Air	0.044	1.84	9.4	0.91	0.54	0.59	±0.01	0.32	6.2	
hdr629-2	Amorphous Carbon	Air	0.13	1.84	10.1	0.81	0.50	0.57	±0.03	0.29	[a]	
hdr630-0	Amorphous Carbon	Air	0.436	1.84	15.2	1.23	0.67	0.54	±0.02	0.27	9.8	
hdr630-1	Amorphous Carbon	Air	0.872	1.84	16.8	1.18	0.65	0.28	±0.01	0.15	8.4	
hdr639-0	Amorphous Carbon	Air	1.3	1.95	25.9	1.14	0.57	0.21	±0.01	0.11	9.2	
hvr2187	Graphite	Air	1.3	0.47	103.7	[b]	–	0.04	±0.02	0.09	[a]	
hvr2188	Graphite	Air	1.3	0.48	102.7	[b]	–	0.04	±0.01	0.08		
hvr2189	Graphite	Air	1.3	0.66	118.6	[b]	–	0.06	±0.05	0.09		
hvr2190	Graphite	Air	1.3	0.87	94.1	[b]	–	0.1	±0.01	0.10		
hvr2191	Graphite	Air	1.3	0.95	68.6	[b]	–	0.11	±0.02	0.11		
hvr2192	Graphite	Air	1.3	1.3	67.5	[b]	–	0.13	±0.01	0.10	–	
hvr2193	Graphite	Air	1.3	1.28	84.9	[b]	–	0.13	±0.02	0.10	–	
hvr2194	Graphite	Air	1.3	1.62	78.9	[b]	–	0.16	±0.02	0.10	–	
hvr2197	Graphite	Air	1.3	1.58	58.8	[b]	–	0.17	±0.01	0.11	–	
hvr2199	Graphite	Air	1.3	2.1	47.7	[b]	–	0.26	±0.03	0.12	–	
hvr2200	Graphite	Air	1.3	2.04	65.7	[b]	–	0.21	±0.02	0.10	–	
hvr2201	Graphite	Air	1.3	2.44	40.7	[b]	–	0.25	±0.04	0.10	–	
hvr2202	Graphite	Air	1.3	2.48	60.7	[b]	–	0.26	±0.05	0.10	–	
hvr2198	Amorphous Carbon	Air	1.3	1.84	22.0	1.13	0.61	–	–	–	[a]	[c]
hvr2203	Amorphous Carbon	Air	1.3	2.84	17.6	1.69	0.60	0.42	±0.05	0.16	5.43	
hvr2204	Amorphous Carbon	Air	1.3	0.74	62.5	0.47	0.61	0.1	±0.03	0.15	28.6	
hvr2205	Amorphous Carbon	Air	1.3	0.74	57.7	0.48	0.65	0.07	±0.03	0.09	25.1	[c]
hvr2209	Amorphous Carbon	Air	1.3	2.0	23.9	1.29	0.63	0.3	±0.04	0.15	4.4	CO2 monitaring (Max: 2894 ppm)

TC: Temperature measurement by thermocouple.

[a] D_c was not well defined due to the noise on shear, gouge leakage or overall gradual weakening during experiment.

[b] Peak friction was not recognised.

[c] Experiment was stopped during weakening.

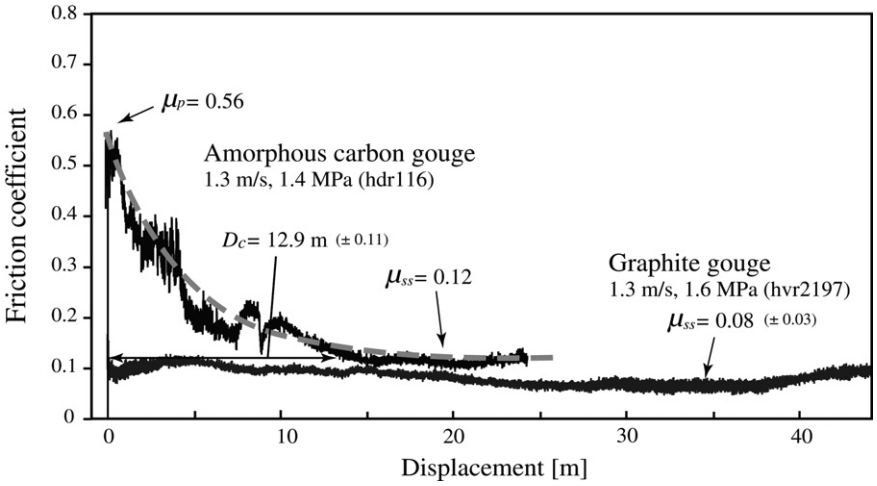

Fig. 3. Representative frictional behavior of amorphous carbon (black line) and graphite gouge (gray line) at a slip rate of 1.3 m/s and normal stresses of 1.4 MPa (amorphous carbon) and 1.6 MPa (graphite). Dashed line is a least-squares fit to the slip-weakening behavior with an empirical equation (Eq. (1)).

Amorphous carbon exhibits dramatic, nearly exponential slip-weakening at all normal stresses (Fig. 4a), with peak and steady-state friction coefficients of 0.54 and 0.15, respectively, neglecting very small cohesion terms (Fig. 4c; see linear equations fit to the data). This friction coefficient is lower than that for most rocks compiled by Byerlee (1978). Slip-weakening distance D_c decreases from about 25 m to 6 m as the normal stress σ_n increases from 0.8 to 2.8 MPa (Fig. 4e). On the other hand, graphite shows low friction throughout the tests (Fig. 4b) with the friction coefficient of 0.11 (Fig. 4d).

3.2. Velocity dependence of friction

Peak friction coefficient of amorphous carbon is about 0.55 at all slip rates. But the steady-state friction coefficient decreases from 0.51 to 0.1 as the slip rate increases from 0.04 to 1.3 m/s (Fig. 5a), whereas it remains nearly the same (about 0.55) at low slip rates (50 μm/s to 5 mm/s) with no slip-weakening (Fig. 5c). On the other hand, friction coefficient of graphite is low (about 0.1) and remains about the same all throughout the tests (Fig. 5b and d). This result is comparable to the friction coefficient reported by Moore and Lockner (2004) using a triaxial deformation apparatus at low slip rate (5 μm/s).

Plots for frictional coefficients at all slip rates clearly indicate that slip-weakening of amorphous carbon gouge begins to occur at slip rate of around 10^{-2} m/s and that its steady-state friction reduces to the same level (0.1) as that of graphite at slip rate of about 1 m/s (Fig. 6). However, the peak friction μ_p did not exhibit velocity weakening, remaining at 0.58 ± 0.08 throughout the velocity range from centimeters to meters per second (open circles in Fig. 6). Graphite gouge had a very low friction coefficient ($\mu < 0.2$) over a range of more than five orders of magnitude in slip rate (filled squares in Fig. 6).

3.3. Experiments for atmospheric and N_2 purged conditions

We found no significant difference in the mechanical behavior of amorphous carbon gouge sheared under atmospheric (Fig. 4a) and N_2 purged, anoxic environments at high slip rates (Fig. 7a). In amorphous carbon gouge deformed at a slip rate of 1.3 m/s and normal stress of 2.0 MPa in air, the emission of CO_2 gas was detected (2894 ppm maximum) at 2.4 s after the onset of experiment, and its concentration increased continuously with displacement (Fig. 7b). We also detected emission of CO_2 from graphite gouge (in trial hvr1555, not shown in Fig. 7), although the CO_2 concentration was over two orders of magnitude less (approximately 40 ppm at the maximum). This result suggests that although carbonaceous material emits CO_2 gas during seismic fault motion, the CO_2 concentration depends strongly on the crystallinity of the material.

4. Fault zone microstructures and mineralogical analysis

All high-velocity experiments on amorphous carbon and graphite resulted in the development of shiny slickenside surfaces between the rotational-side of dolerite host rock and the gouge zone. Less shiny slickenside surfaces were also recognized for specimens deformed at low slip rates. Microscope and SEM (scanning electron microscope) observations on a thin section (see Fig. 2 for orientation) reveal a slip zone of about 65 μm in width of amorphous carbon deformed at a slip rate v of 1.3 m/s and at a normal stress σ_n of 1.0 MPa (Fig. 8a; reflected light image). The slip zone is more compacted and appears bright colored. Almost no grain size reduction and fabric development are recognized in the weakly deformed zone. Observation of graphite gouge deformed at v = 0.04 m/s and σ_n = 1.0 MPa in a thin section with a similar orientation reveal a well-compacted slip zone of about 50 μm in width (Fig. 8b; reflected light image). In the weakly deformed zone, grain size is unchanged, but weak foliation forms.

Slickenside surfaces in amorphous carbon (Fig. 8c; sheared at v = 1.3 m/s and σ_n = 1.0 MPa) and graphite (Fig. 8d; sheared at v = 1.3 m/s and σ_n = 1.0 MPa) are smooth surfaces with fine grooves formed parallel to the slip direction. Fine carbon particles of micrometers to sub-micrometer sizes constitute the slickenside surface of amorphous carbon (Fig. 8c) and those grains are finer than the grains in weakly deformed zone immediately underneath the surface (Fig. 8d). Most experiments on amorphous carbon were conducted in air and some carbon along the slip surface must have disappeared by oxidation transforming to CO_2 (Fig. 7b). On the other hand, larger grains of several tens of micrometers in size can be recognized on the slickenside surface of graphite (inset of Fig. 8d) and texture suggests that platy graphite grains are aligned nearly parallel to the surface. Graphite has a well-known sheet structure (e.g., Inagaki and Kang, 2006), so that graphite grains seem to have rotated without much grain crushing to form foliation.

To examine the mineralogical changes during high-velocity experiments in a N_2 atmosphere, XRD (X-ray powder diffraction)

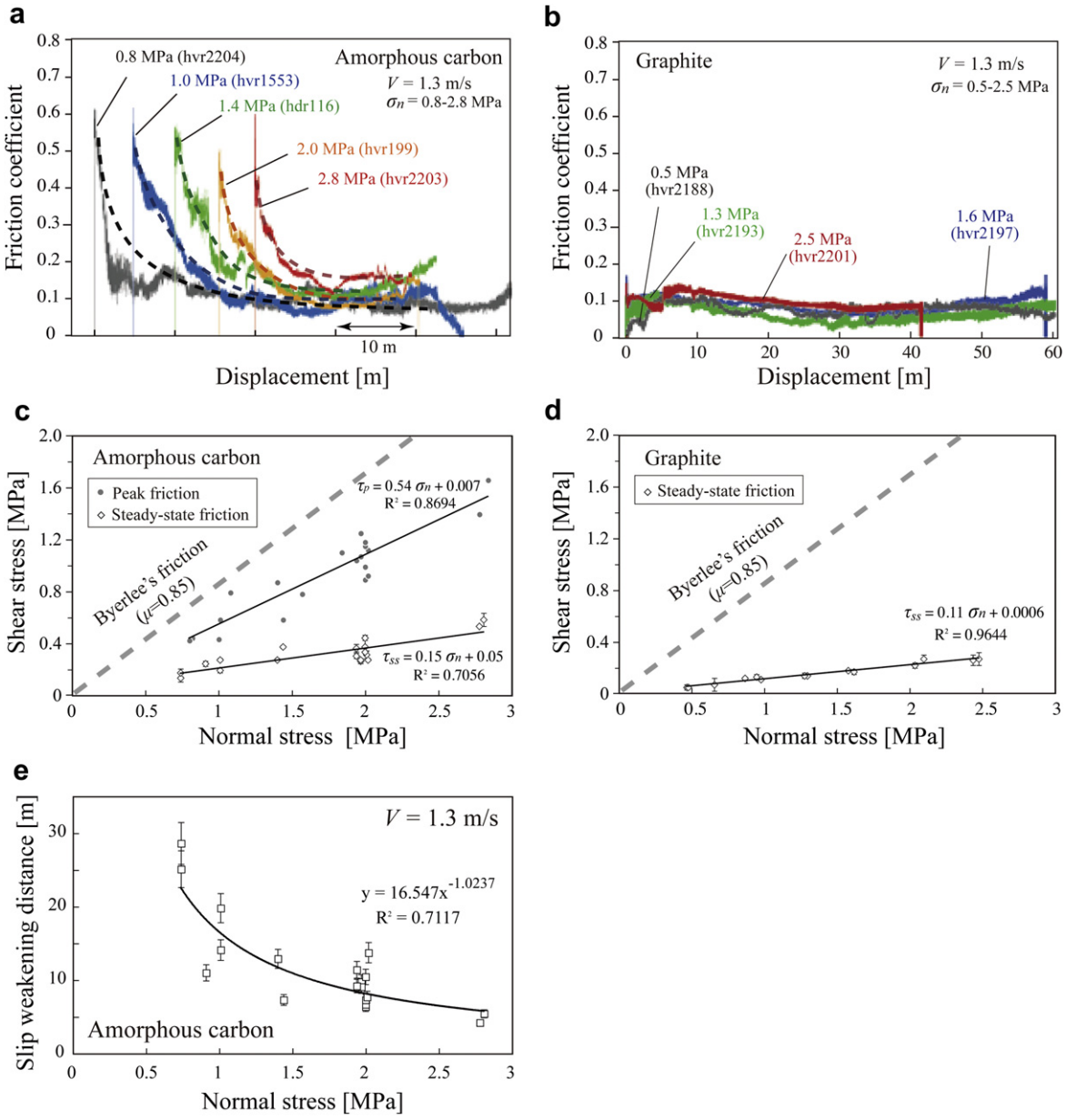

Fig. 4. Frictional behavior at various normal stresses of amorphous carbon gouge (a) and graphite gouge (b) at a slip rate of 1.3 m/s. Dashed lines in (a) are least-squares fitting curves with Eq. (1), and the five trials are shown offset by 5 m for visibility. Shear stress is plotted against normal stress at peak and steady-state friction for amorphous carbon gouge (c) and steady-state friction for graphite gouge (d) at a slip rate of 1.3 m/s. Byerlee's law ($\tau = 0.85\sigma_n$) is shown as a dashed line for comparison. (e) Slip-weakening distance D_c plotted against σ_n for amorphous carbon gouge at a slip rate of 1.3 m/s. The solid line is a power-law relationship fitting the data.

analysis was performed on material from both the slip zone and the weakly deformed zone. XRD analyses were performed on a Rigaku MultiFlex-2kW apparatus with the following measurement conditions: Cu–Kα radiation, X-ray generator at 40 kV, 40 mA, scanning step 0.02, scanning speed 2/min, divergence slit 1°, scattering slit 1° and receiving slit 0.15 mm. A sample from the slip zone of amorphous carbon deformed in N_2 purged atmosphere at a slip rate of 1.3 m/s displays a diffraction peak at 3.3 Å corresponding to the spacing distance on the graphite (002) plane (upper curve in Fig. 9a), whereas no diffraction peaks are seen in samples of the starting amorphous carbon (the bottom curve in the same figure). A sample from weakly deformed zone of the same specimen shows a small diffraction peak at about the same place (second curve from the top in Fig. 9a). It is well known that the spacing distance of the (002) crystal surface in carbonaceous material, d_{002}, becomes small with increasing crystallinity (e.g., Landis, 1971; Inagaki and Kang, 2006). The d_{002} values of the slip zone materials were always smaller than those of the weakly deformed zone (see Table 1), approaching the ideal (002) spacing of graphite (3.335 Å) with increasing displacement, and peak intensity also tended to increase with displacement (Fig. 9b). In contrast, no diffraction peak was found in the experiments in air even in the slip zone (hdr125 in Fig. 9a), graphitization did not take place after rapid slip in oxic conditions. Additionally, the clear diffraction peak of the graphite was hardly detected from the slip zone samples deformed at low to intermediate slip rates to displacement of 20–36.5 m (hdr066, hvr2264 in Fig. 9a).

We performed TEM (transmission electron microscope) observation for the amorphous carbon gouge prior and after the

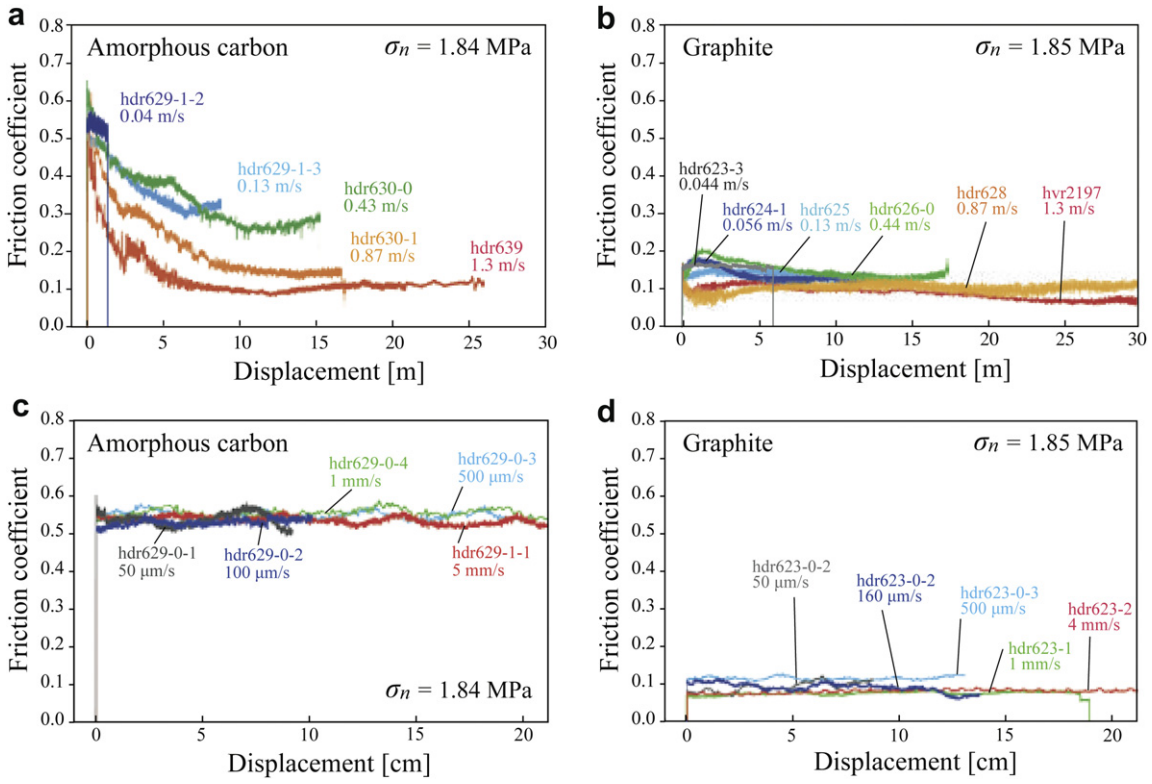

Fig. 5. Frictional behaviors at various slip rates on amorphous carbon gouge (a, c) and graphite gouge (b, d) at a normal stress of ~1.8 MPa in an intermediate to high-velocity regime (slip rate of 0.04–1.3 m/s) (a, b) and a low to intermediate-velocity regime (slip rate of 50 μm/s to 5 mm/s) (c, d).

high-velocity friction experiment. A JEOL JEM-2010 high-resolution TEM equipped with an energy dispersive spectrometer under an accelerating voltage of 200 kV is used for observation. For preparation of TEM specimens, gouge powder was suspended in ethanol, then dropped onto a copper microgrid with elastic substrate without carbon coating. Under the TEM, the starting material showed typical amorphous textures throughout the specimen (maze pattern, Fig. 10a). In contrast, the same materials in the slip zone underwent high-velocity friction experiment displayed particles with characteristic lattice fringes (Fig. 10b) that resemble those of graphite formed by heat treatment of coke at 1100–1300 °C (Inagaki and Kang, 2006). Thus, both XRD and TEM analyses clearly indicate that graphitization of amorphous carbon occurred only at high slip rates in the N_2 environment.

5. Interpretation and discussion

5.1. Thermal oxidation of carbonaceous minerals

In our experiments in air, emission of CO_2 gas was detected immediately after the onset of sliding. One possible source of CO_2 is carbonates in the gouge, and CO_2 degassing has been reported in

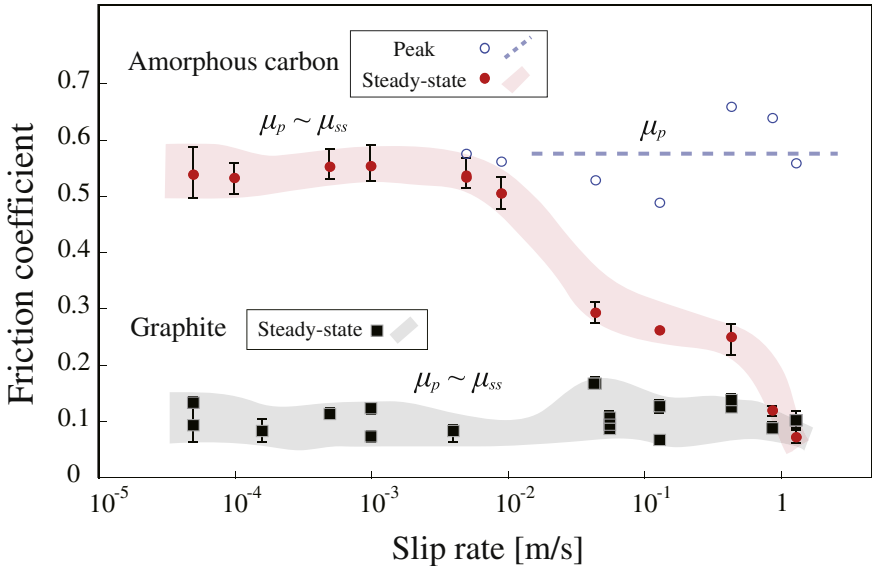

Fig. 6. Peak and steady-state friction plotted against slip rate for amorphous carbon (open and solid circles) and graphite gouge (squares).

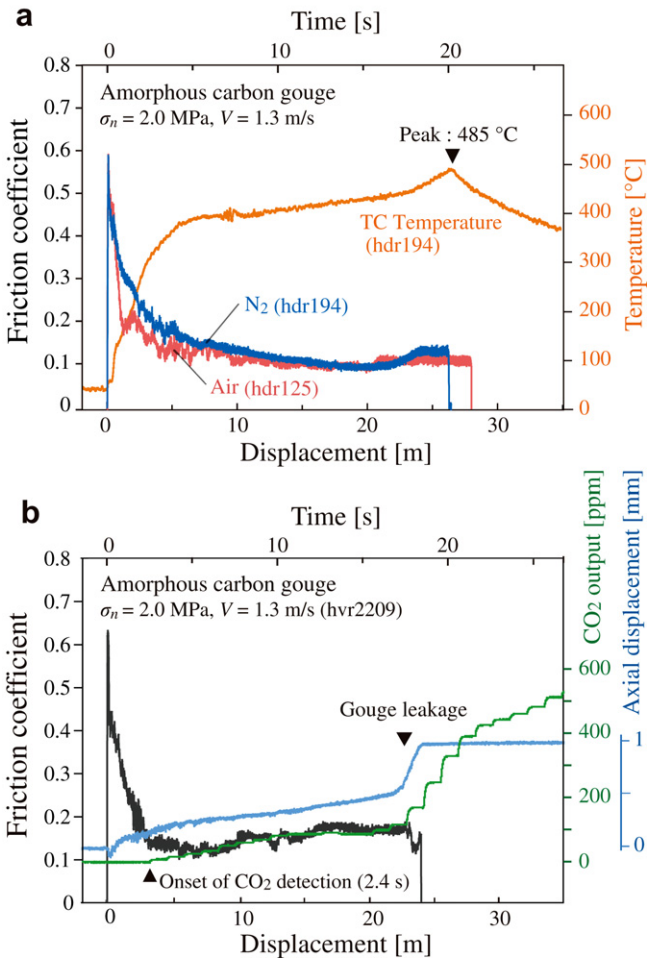

Fig. 7. (a) Mechanical data of amorphous carbon gouge under oxic (air) and anoxic (N_2) environments at a slip rate of 1.3 m/s and normal stress of 2.0 MPa (hdr125 and hdr194, respectively). Temperature near sliding surface measured by thermocouple is also shown by orange line (run hdr194). (b) Representative mechanical data at same conditions as those in (a), plus axial shortening of gouge zone thickness and CO_2 concentration in the specimen chamber. (For interpretation of the references to colour in this figure legend, the reader is referred to the web version of this article).

similar experiments on calcite, siderite, and dolomite (Han et al., 2007a,b; De Paola et al., 2011). However, we used pure amorphous carbon and graphite powders as starting materials, and the host rock dolerite did not show any patterns typical of carbonates in XRD measurements. It is well known that amorphous carbon and graphite starts to react with oxygen (thermal oxidation reaction) at about 300–400 °C and 450–500 °C, respectively, in an oxic environment (Boylan, 1996; Xiaowei et al., 2004):

$$C + O_2 \rightarrow CO_2 \quad (2)$$

Thermocouples placed 0.03 mm from the sliding surface showed that the temperature reached 300 °C within 2–3 s after the onset of sliding (Fig. 7a), which is high enough to trigger thermal oxidation. The time of the first emission of CO_2 is nearly consistent with the time at which 300 °C was reached (Fig. 7a and b), strongly supporting thermal oxidation.

Our experiments demonstrated that frictional heating by rapid coseismic sliding induces immediate oxidization of carbon minerals in fault zones under oxic conditions typical of shallow crustal depths. CO_2 gas emission has been observed along natural faults (e.g., the Atotsugawa fault; Saito et al., 2006) and is considered to result from dissolution of carbonate rocks, volcanic gas, and organic soil compounds. Our results suggest that thermal oxidation of carbonaceous minerals is another possible source of CO_2 gas along natural faults, especially in carbon-rich sedimentary rocks (e.g., inland or forearc basins and accretionary prisms) if oxic environments are present in fault zones.

5.2. Graphitization of amorphous carbon and geological evidence of seismic fault motion

In our experiments under an N_2 environment, amorphous carbon did not oxidize into CO_2 but underwent partial graphitization (Figs. 9a and 10b). Graphitization occurs for (1) static heating at 1000–2200 °C (Oberlin, 1984), (2) heating at 500 °C under 0.6 GPa pressure for more than 1 month (Nover and Stoll, 2001), (3) simple shear deformation at pressures of 0.8–1.0 GPa, a temperature of 900 °C, and a duration of a few to hundreds of hours (Wilks et al., 1993; Bustin et al., 1995), and (4) temperatures of 300–500 °C at pressures of 0.4–0.5 GPa over geologic time (e.g., Diessel et al., 1978; Buseck and Huang, 1985). However, none of these conditions were met in our high-velocity experiments with an applied normal stress of <3 MPa, temperatures <500 °C, and duration of less than hundreds of seconds.

One possible cause of graphitization during our high-velocity experiments is flash heating at microscopic asperity contacts of gouge particles (Archard, 1958/1959). Although the original theory of flash heating assumed sliding asperities on two parallel planes, the concept also could be applied to the microscopic contacts between gouge particles being sheared within a narrow slip zone. Flash temperature (T_f) at the asperity contacts is estimated by the equation:

$$T_f = 0.25\beta(\mu\pi P_m/\rho C_p)(aV/2\kappa) \quad (3)$$

where the dimensionless Peclet number, $L = aV/2\kappa$, is between 0.1 and 0.5, β is an empirical constant of 0.95, μ is friction coefficient, P_m is yield strength, a is asperity contact radius, V is slip rate, κ is thermal diffusivity, ρ is density, and C_p is heat capacity. The material properties of amorphous carbon used for the estimates are: $\rho = 2000$ kg/m^3, $C_p = 710$ J/kg K, $\kappa = 6.5 \times 10^{-6}$ m^2/s, and $P_m = 2$ GPa (estimated by converting the Shore hardness of 100–120 (Inagaki and Kang, 2006) to the indentation hardness). In the case of $a = 2$ μm based on the SEM observation, $\mu = 0.17$ and $V = 1.3$ m/s, the estimated flash temperature is 50.5 °C. Thus, the maximum temperature expected at the asperity contacts at the steady-state, which is the summation of background temperature (i.e. temperature measured by thermocouples in Fig. 7a) and flash temperature, is estimated to be ~600 °C. Although flash temperature rise is not so large due to the low yield strength of amorphous carbon in our experiments, flash temperature rise may affect the graphitization. In addition, stress concentration at asperity contacts of gouge particles also yields short-lived high stresses (a few GPa) that may contribute to graphitization.

Another possible cause of graphitization is shear strain (Wilks et al., 1993; Bustin et al., 1995), which in our case was more than 10,000. Although it is not clear which effect might predominate, both thermal and mechanical forces at asperity contacts must contribute to graphitization during high-velocity experiments under anoxic conditions. This explanation is consistent with the graphitization observed only within the slip zones sheared at high slip rates (Fig. 9a) and with the partial graphitization observed only at possible rims of amorphous carbon grains under the TEM (Fig. 10b). In the case of oxic conditions, thermal oxidation takes place prior to the graphitization and the amorphous carbon

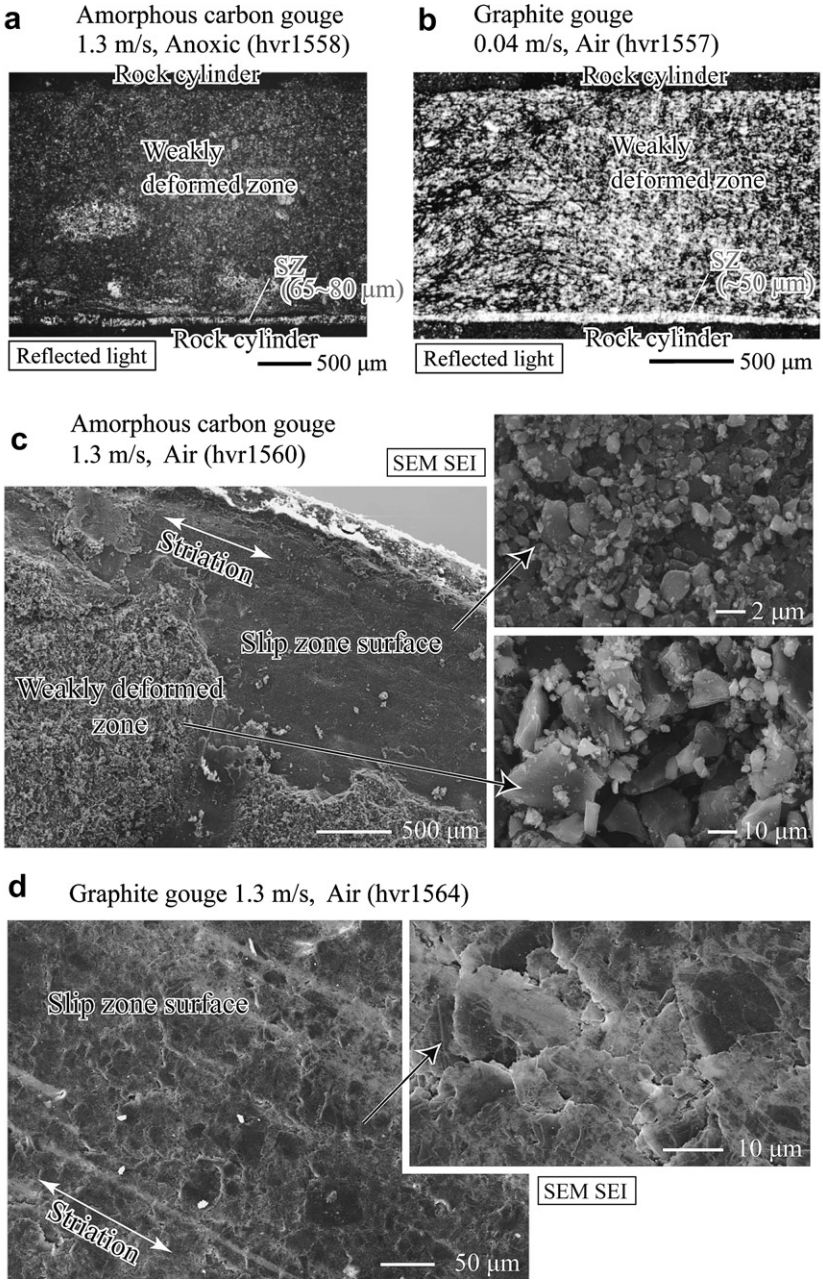

Fig. 8. Reflected light micrographs of thin section of amorphous carbon (a) and graphite gouges (b). (a) Amorphous carbon gouge sheared at a slip rate of 1.3 m/s and normal stress of 1.0 MPa under anoxic condition, showing a slip zone (SZ) 65 ~ 80 μm thick between the rock cylinder and gouge zone that corresponds to the cohesive thin layer. (b) Graphite gouge sheared at a slip rate of 0.04 m/s and normal stress of 1.0 MPa, showing a slip zone ~50 μm thick between the rock cylinder and gouge zone. (c) SEM secondary electron images of slip surface and weakly deformed zone of amorphous carbon gouge sheared at a slip rate of 1.3 m/s and normal stress of 1.0 MPa. Upper and lower insets show magnification of slip zone and weakly deformed zone, respectively. Grain size reduction (down to a few micrometers to sub-micrometer in diameter) and increase of roundness are observed from slip surface. (d) SEM secondary electron images of slip surface of graphite gouge sheared at a slip rate of 1.3 m/s and normal stress of 1.0 MPa. The inset shows magnification of slip zone. Preferably oriented graphite particles making very smooth slickenside.

transforms into CO_2 gas. This behavior is why the graphitization of the amorphous carbon could not be found in the sample deformed under oxic conditions.

The transformation of carbonaceous minerals by thermal oxidation (in oxic conditions) and graphitization (in anoxic conditions) may leave geological records, as carbonaceous material is chemically stable and not prone to dissolution. For example, by observing thin continuous graphite-rich layers within a fault zone composed of low crystallinity carbon, one could infer that the graphite formed during seismogenic fault motion. If carbonaceous minerals are missing in a slip zone within a fault zone containing carbonaceous minerals, the zone was likely subjected to seismogenic fault motion under oxic conditions near the ground surface. Based on such evidence, we identified G1′ in Fig. 1 in the Tanakura fault as the principal slip zone during past seismogenic fault motion at depths. Identification of slip zones which accommodated fault motion is not always easy, but such changes in carbonaceous minerals may lead to a way of identifying coseismic slip zones in natural fault systems.

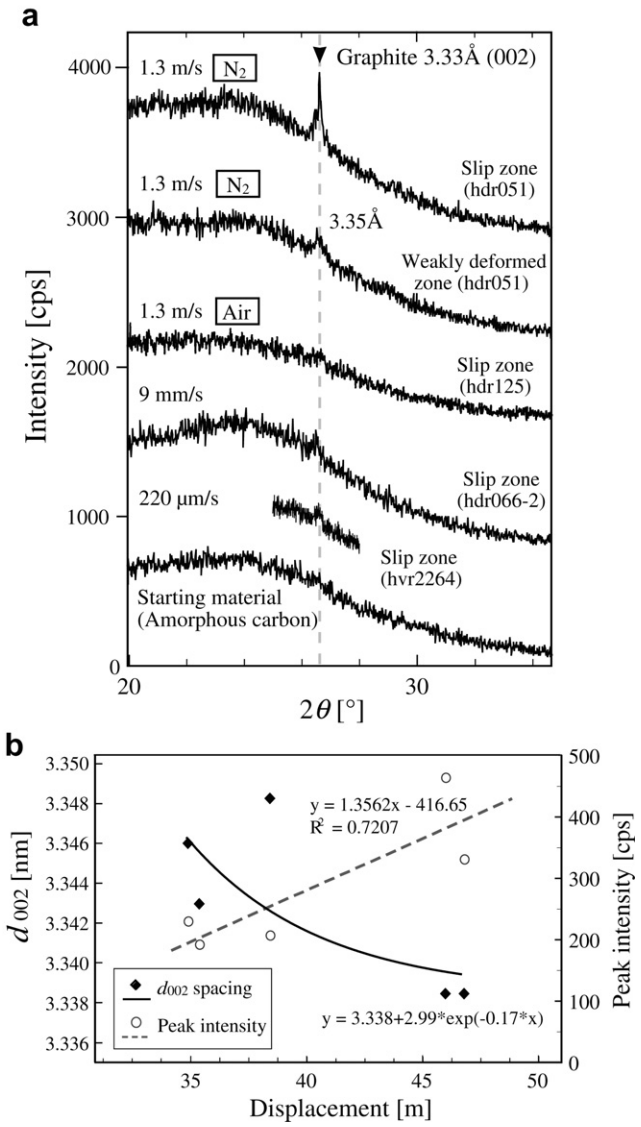

Fig. 9. (a) Representative X-ray diffraction patterns of amorphous carbon gouge before and after experiments at slip rates of 220 μm/s, 9 mm/s and 1.3 m/s in air and N_2 atmospheres. Graphite (002) diffraction (3.33 Å) is only recognized on recovered material sheared at a slip rate of 1.3 m/s in the N_2 atmosphere. For recovered sample of hvr2264, measurement was done only from 25 to 28° of theta angle. Patterns are offset for visibility. (b) Evolution of peak position and peak intensity of graphite (002) diffraction in slip zone material with increasing displacement. All experiments are conducted at slip rate of 1.3 m/s. The d_{002} spacing (solid line) decreases exponentially toward the 3.338 Å closely ideal d_{002} spacing of graphite (3.335 Å).

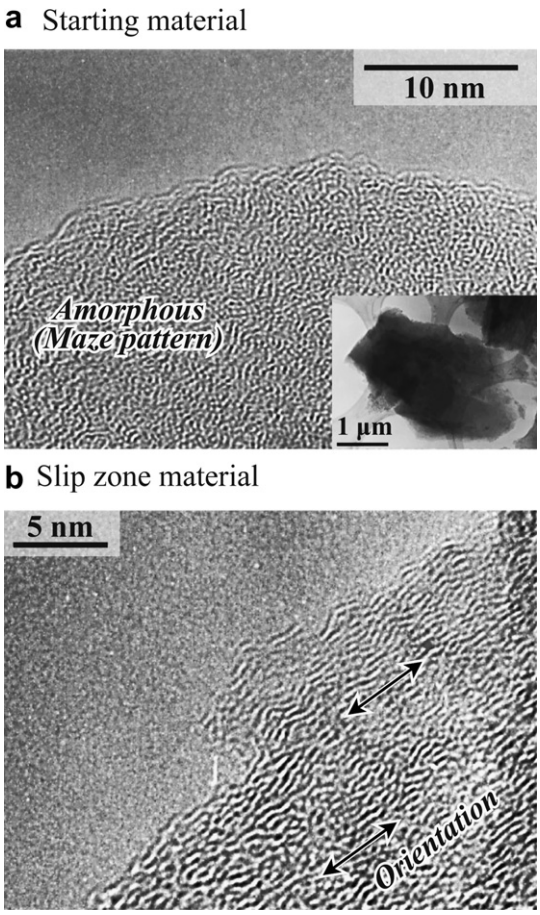

Fig. 10. TEM images of amorphous carbon starting material (a) and slip zone material recovered from an experiment at a slip rate of 1.3 m/s in the N_2 atmosphere; hdr051 (b).

5.3. Implications for presence of graphite and amorphous carbon on fault mechanics

Graphite is well known for its use as a solid lubricant, and in our experiments the friction coefficient of graphite powder was very low over a wide range of slip rates whereas that of amorphous carbon became low only at slip rates greater than a few centimeters per second, similar to other rock-forming minerals (Wibberley et al., 2008). These results have important implications for earthquake geology and fault mechanics. In general, carbonaceous materials are ubiquitous in pelitic rocks in sedimentary basins, metamorphic belts or accretionary complexes. Fault zones in such tectonic regions are often enriched with carbonaceous minerals (Zulauf et al., 1990; Manatschal, 1999; Awaji, 2006; Oohashi and Kobayashi, 2008). Once rapid faulting occurs within such a fault zone at anoxic depths, the fault could become dramatically weak or slippery at all slip rates due to the generation of graphite by coseismic faulting. This weakening is effective at depths where potentially stable minerals, such as smectite (Saffer and Marone, 2003), could not exist anymore. If graphite is widespread, with the development of continuous and/or interconnected layers of graphite within the fault zones, a long-term weak fault zone (Holdsworth, 2004; Collettini et al., 2009) may be created, because graphite is weak at the wide range of slip velocities (Fig. 6). How effective this lubrication becomes, depends on the graphite content and slip zone structures.

High-velocity friction experiments have demonstrated dramatic weakening of faults without frictional melting at slip rates greater than the order of 10 mm/s (e.g., Di Toro et al., 2004; Han et al., 2007a; Hirose and Bystricky, 2007; Mizoguchi et al., 2009). Surprisingly, the overall behavior of amorphous carbon is quite similar to those behaviors; i.e., fairly high friction at low to intermediate slip rates, but dramatic weakening at high slip rates. Amorphous materials have received attention since they forms during frictional sliding (Yund et al., 1990) and silica gel, a form of amorphous materials, is proposed to cause such weakening (Goldsby and Tullis, 2002; Di Toro et al., 2004). Previous experiments are inconclusive in this regard since amorphous materials form during frictional slip and may not be controlling the entire behavior. We did use amorphous carbon as the starting material, and given that the host rock dolerite is stronger, we believe that the amorphous carbon is likely to control the overall behavior. Friction experiments using a variety of amorphous materials from rocks are needed to resolve this important issue.

6. Conclusions

The main conclusions of our experimental study are

1. For amorphous carbon sheared at 1.3 m/s, the friction coefficient rapidly increased to ~0.54 at the initiation of slip, then decreased exponentially with displacement toward a steady-state friction coefficient of ~0.15. On the other hand, graphite gouge sheared at 1.3 m/s showed a nearly constant friction coefficient of ~0.08 without visible slip-weakening or strengthening throughout the experiment. For slip rates from 50 μm/s to 5 mm/s, friction coefficients of amorphous carbon and graphite gouges exhibited nearly constant values of 0.54 ± 0.04 and 0.10 ± 0.03, respectively. Thus, friction of graphite gouge was very low throughout the range of our velocity conditions (50 μm/s to 1.3 m/s).
2. Graphitization (crystallization) of amorphous carbon was recognized in the slip zone, which underwent frictional heating due to rapid sliding. XRD analyses and TEM observations suggest that thermally and mechanically driven mineral transformation at asperity contacts contributes to graphitization during high-velocity experiments under anoxic conditions. Therefore, graphitization of amorphous carbon may be a possible indicator of paleoseismic faulting, as carbonaceous minerals are chemically stable on a geologic timescale at anoxic depths.
3. Once rapid faulting occurs within the carbon-rich, anoxic fault zones that typically occur in accretionary complexes, fault might become slippery by the generation of graphite. The presence of graphite could contribute to slow deformation, such as slow slip events observed along subduction zones, as graphite shows low friction over the wide range of slip rates. Thus, mineralogical transformation of carbonaceous minerals by rapid faulting may play an important role in fault behavior at seismogenic depths. Carbonaceous materials can be oxidized in oxic environments and be a source of CO_2 in fault zones.
4. Gouge composed of amorphous carbon exhibits frictional behaviors quite similar to those of natural fault gouges (i.e. Nojima fault gouge; Mizoguchi et al., 2007), middle to high friction at low to intermediate slip rates, but dramatic high-velocity weakening. Amorphous gouge was often found in the slip localization zones recovered after high-velocity experiments (e.g., Brantut et al., 2008), and hence, amorphous materials may generally cause such velocity weakening behaviors.

Acknowledgments

We thank Dr. Raehee Han and Dr. Jun-ichi Ando for constructive discussion and technical help. Constructive reviews by Anne-Marie Boullier and Cristiano Collettini are greatly appreciated. This work was supported by a Grant-in-Aid for JSPS fellows (21-04493) and a Grant-in-Aid for Young Scientists (B) (20740264), Japan Society for Promotion of Science. Transmission electron microscope work was done at the Natural Science Center for Basic Research and Development (N-BARD), Hiroshima University.

Appendix A. Evaluation of the effect of the Teflon sleeve on frictional behavior

In this study, we used a Teflon sleeve to surround the simulated fault zone and prevent leakage of gouge material. We evaluated the friction at the contact between the Teflon sleeve and the outer surface of the host rock in experiments without gouge to determine the corrections needed to the mechanical data. Experiments were performed with an empty space 1 mm wide between the rotary and stationary cylinders at various slip rates and zero normal stress (see Fig. A1). On the runs at slip rates >56 mm/s, typical slip-weakening behavior was observed (Fig. A1b and c), with measured shear tractions at initial peak and steady-state of ~0.75 Nm and 0.1–0.4 Nm, respectively. At the lowest slip rate of 0.15 mm/s, the shear traction fluctuated between 0.5 and 0.75 Nm. When the normal stress applied to the gouge was 1 MPa, Teflon friction contributed ~18% and <8% to the measured shear traction at the initial peak and steady-state, respectively. The contribution of Teflon friction decreased at higher applied normal stress. To determine intrinsic frictional behavior, we subtracted the shear traction obtained from the experiments without gouge from the raw traction data from each gouge experiment. Slight fluctuations of the friction coefficient after making the Teflon correction can be attributed to gouge leakage and tilting or movement of the Teflon sleeve, because the sleeve was not fixed during the experiments.

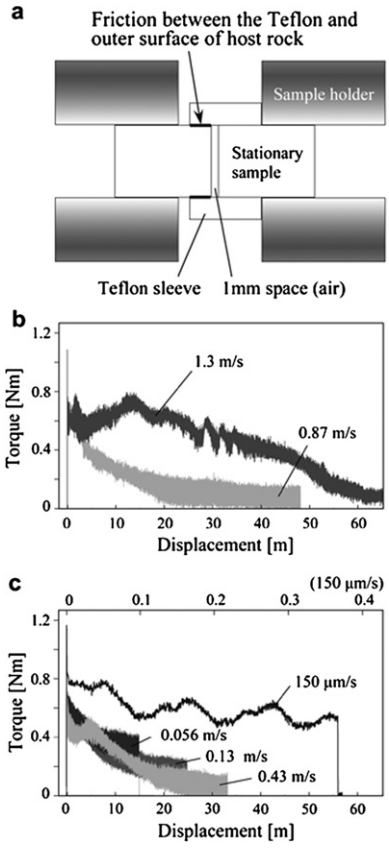

Fig. A1. (a) Schematic specimen configuration for the gougeless experiment to evaluate the effect of Teflon friction. Frictional behavior of Teflon sleeve is shown at high (b) and low to intermediate-velocities (c).

References

Archard, J.F., 1958/1959. The temperature of rubbing surfaces. Wear 2, 438–455.
Awaji, D., 2006. Relationship between kinematic history and formation process of fluid channel in brittle shear zone. PhD Thesis. Waseda University, Japan, pp. 104 (in Japanese, with English abstract).
Awaji, D., Sugimoto, R., Arai, H., Kobayashi, K., Takagi, H., 2010. Miocene dextral movement of Tanakura shear zone: evidence from the western marginal fault, Hanawa Town, northeast Japan. Island Arc 19, 561–564.
Boylan, J., 1996. Smooth operators: carbon–graphite materials. Material World 4, 707–708.
Brantut, N., Schubnel, A., Rouzaud, J.-N., Brunet, F., Shimamoto, T., 2008. High velocity frictional properties of a clay-bearing fault gouge and implications for earthquake mechanics. Journal of Geophysical Research 113 (B10401). doi:10.1029/2007JB005551.
Buseck, P.R., Huang, B.-J., 1985. Conversion of carbonaceous material to graphite during metamorphism. Geochimica et Cosmochimica Acta 49, 2003–2016.

Bustin, R.M., Ross, J.V., Rouzaud, J.N., 1995. Mechanism of graphite formation from kerogen: experimental evidence. International Journal of Coal Geology 28, 1–36.
Byerlee, J.D., 1978. Friction of rocks. Pure and Applied Geophysics 116, 615–626.
Collettini, C., Niemeijer, A., Viti, C., Marone, C., 2009. Fault zone fabric and fault weakness. Nature 462, 907–910. doi:10.1038/nature08585.
De Paola, N., Hirose, T., Mitchell, T.M., Di Toro, G., Viti, C., Shimamoto, T., 2011. Fault lubrication and earthquake propagation in thermally unstable rocks. Geology 39, 35–38. doi:10.1130/G31398.1.
Di Toro, G., Goldsby, D.L., Tullis, T.E., 2004. Friction falls toward zero in quartz rock as slip velocity approaches seismic rates. Nature 427, 436–439. doi:10.1038/nature02249.
Diessel, C.F.K., Brothers, N.R., Black, P.M., 1978. Coalification and graphitization in high-pressure schists in New Caledonia. Contributions to Mineralogy and Petrology 68, 63–78.
Goldsby, D.L., Tullis, T.E., 2002. Low frictional strength of quartz rocks at subseismic slip rates. Geophysical Research Letters 29 (17), 1844. doi:10.1029/2002GL015240.
Han, R., Shimamoto, T., Hirose, T., Ree, J., Ando, J., 2007a. Ultralow friction of carbonate faults caused by thermal decomposition. Science 316, 878–881.
Han, R., Shimamoto, T., Ando, J., Ree, J., 2007b. Seismic slip record in carbonate-bearing fault zones: an insight from high-velocity friction experiments on siderite gouge. Geology 35, 1131–1134.
Hirose, T., Bystricky, M., 2007. Extreme dynamic weakening of faults during dehydration by coseismic shear heating. Geophysical Research Letters 34 (L14311). doi:10.1029/2007GL030049.
Hirose, T., Shimamoto, T., 2005. Growth of molten zone as a mechanism of slip weakening of simulated faults in gabbro during frictional melting. Journal of Geophysical Research 110 (B05202). doi:10.1029/2004JB003207.
Holdsworth, R.E., 2004. Weak faults–rotten cores. Science 303, 181–182. doi:10.1126/science.1092491.
Inagaki, M., Kang, F., 2006. Carbon Materials Science and Engineering: From Fundamentals to Applications. Tsinghua University Press, pp. 604.
Itaya, T., 1981. Carbonaceous material in pelitic schists of the Sanbagawa metamorphic belt in central Shikoku, Japan. Lithos 14, 215–224.
Landis, C.A., 1971. Graphitization of dispersed carbonaceous material in metamorphic rocks. Contributions to Mineralogy and Petrology 30, 34–45.
Manatschal, G., 1999. Fluid and reaction assisted low angle normal faulting: evidence from rift related brittle fault rocks in the Alps (Err Nappe, eastern Switzerland). Journal of Structural Geology 21, 777–793.
Mizoguchi, K., Hirose, T., Shimamoto, T., Fukuyama, E., 2007. Reconstruction of seismic faulting by high-velocity friction experiments: an example of the 1995 Kobe earthquake. Geophysical Research Letters 34 (L01308). doi:10.1029/2006GL027931.
Mizoguchi, K., Hirose, T., Shimamoto, T., Fukuyama, E., 2009. High-velocity frictional behavior and microstructure evolution of fault gouge obtained from Nojima fault, southwest Japan. Tectonophysics. doi:10.1016/j.tecto.2009.02.033.
Moore, D.E., Lockner, D.A., 2004. Crystallographic controls on the frictional behavior of dry and water-saturated sheet structure minerals. Journal of Geophysical Research 109 (B03401). doi:10.1029/2003JB002582.
Nover, G., Stoll, J., 2001. Graphitisation of carbon – a p, T-laboratory experiment. In: Hördt, A., Stoll, J. (Eds.), Protocol on the 19th Colloquium "Electromagnetic Depth Research". German Geophysical Society.
Oberlin, A., 1984. Carbonization and graphitization. Carbon 22, 521–541.
O'Hara, K., Mizoguchi, K., Shimamoto, T., Hower, J.C., 2006. Experimental frictional heating of coal gouge at seismic slip rates: evidence for devolatilization and thermal pressurization of gouge fluids. Tectonophysics 424, 109–118.
Oohashi, K., Kobayashi, K., 2008. Fault geometry and paleo-movement of the central part of the Ushikubi fault, northern central Japan. Journal of the Geological Society of Japan 114, 16–30 (in Japanese, with English abstract).
Saffer, D.M., Marone, C., 2003. Comparison of smectite- and illite-rich gouge frictional properties: implications for the updip limit of the seismogenic zone along subduction megathrusts. Earth and Planetary Science Letters 215, 219–235.
Saito, T., Tanaka, H., Shimada, K., Nakamura, M., 2006. New technology of separating and continuous monitoring of groundwater and desolved gases in 200 m drilled-hole in Atotugawa Fault. In: Japan Geoscience Union Meeting, Abstract S119–006.
Savage, R.H., 1948. Graphite lubrication. Journal of Applied Physics 19. doi:10.1063/1.1697867.
Shimamoto, T., Hirose, T., 2–7 April, 2006. Reproducing Low to High-velocity Fault Motion in Fluid-rich Environments: an Experimental Challenge and Preliminary Results. European Geosciences Union, General Assembly, Vienna, Austria. EGU06-A-09077.
Shimamoto, T., Tsutsumi, A., 1994. A new rotary-shear high-velocity friction testing machine: its basic design and scope of research. Structural Geology 39, 65–78 (in Japanese with English abstract).
Wibberley, C.A.J., Yielding, G., Di Toro, G., 2008. Recent advances in the understanding of fault zone internal structure: a review. In: Wibberley, C.A.J., Kurz, W., Imber, J., Holdsworth, R.E., Collettini, C. (Eds.), The Internal Structure of Fault Zones: Implications for Mechanical and Fluid-Flow Properties. Geological Society, London, Special Publications, vol. 99, pp. 5–33. doi:10.1144/SP299.2.
Wilks, K.R., Mastalerz, M., Ross, J.V., Bustin, R.M., 1993. The effect of experimental deformation on the graphitisation of Pennsylvania anthracite. International Journal of Coal Geology 24, 347–369.
Xiaowei, L., Robin, J.-C., Suyuan, Y., 2004. Effect of temperature on graphite oxidation behavior. Nuclear Engineering and Design 227, 273–280.
Yund, R.A., Blanpied, M.L., Tullis, T.E., Weeks, J.D., 1990. Amorphous material in high strain experimental fault gouges. Journal of Geophysical Research 95, 15589–15602.
Zulauf, G., Kleinschmidt, G., Oncken, G., 1990. Brittle deformation and graphitic cataclasites in the pilot research well KTB-VB (Oberpfalz, FRG). In: Knipe, R.J., Rutter, E.H. (Eds.), Deformation Mechanisms, Rheology and Techtonics. Geological Society, London, Special Publications, vol. 54, pp. 97–103.